JTTEES 1: 169-178

A Pragmatic Analysis and Comparison of HVOF Processes

M.L. Thorpe and H.J. Richter

A number of high-velocity oxygen-fuel flame (HVOF) systems have evolved during the last 9 years. The most advanced is now challenging the coating qualities produced by the very successful detonation (D-Gun) process. The fundamentals of these various processes are described and compared. A mathematical analysis of an established HVOF gun is profiled. Gas and particle temperatures, velocities, pressures, and Mach numbers are calculated and plotted at various points within the gun and spray stream. Significantly, all measured values were in close agreement with calculated and predicted values. Flow patterns and shock-wave phenomena are also described and compared with actual observations.

1. Introduction

MUCH has been written about the high-velocity oxygen-fuel flame (HVOF) thermal spray process. However, a rigorous definition of how this process operates in terms of fundamentals and thermodynamic principles has not yet been established. Therefore, a simple theoretical analysis of the system is proposed to promote a better understanding. In turn, this should allow comparison of experimental data also set forth in this article and enable evaluation of the various designs of HVOF devices.

2. Background

Underlying the entire thermal spray industry is one outstanding coating technique, which has been marketed for decades by Union Carbide and tradenamed D-Gun.[1,2] This process produces premium coatings that have long been the goal of all other coating processes.[1] Many of the advantages of the D-Gun process were obvious; however, it was not possible to duplicate them with other processes. In part, this has been because D-Gun coatings are available only as a service—no equipment for in-plant coating operations has been made available. Consequently, there has been a sparse understanding of just how and why the D-Gun produced superior coatings. Like most inventions, once the fundamental principles are understood, then the reasons for the superior coatings become evident.

A schematic of the D-Gun is shown in Fig. 1, which illustrates how oxygen and fuel gas are mixed with a uniformly dispersed fine powder that is cyclically injected into a shotgun-like barrel at a pressure of 1 atm. A spark ignites the mixture and the pressure rises. Because of the geometry used, the deflagration wave (flame front) is allowed to accelerate to a supersonic detonation wave. This detonation wave propagates and ignites the mixture so rapidly (above the speed of sound) that the pressure in the barrel cannot be relieved (pressure is relieved at the speed of sound). Thus, the well-known detonation phenomenon occurs, namely a significant rise in pressure caused by a rapid, major temperature rise of the burning of fuel/oxygen mixture. A temperature rise of 300 to 3600 K (70 to 6000 °F) occurs with different fuel yielding different temperatures.

Table 1 shows the pressures that may occur from flames and detonations. Note that with the deflagration (common flame) the

Key Words: high-velocity oxygen fuel, particle temperature, particle velocity, shock-wave phenomena, theoretical analysis

M.L. Thorpe, President, Hobart Tafa Technologies, Inc., Concord, New Hampshire, and **H.J. Richter,** Professor of Engineering, Thayer School of Engineering, Dartmouth College, Hanover, New Hampshire.

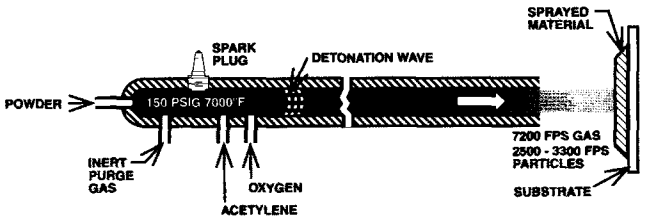

Figure 1 Schematic of D-Gun setup.

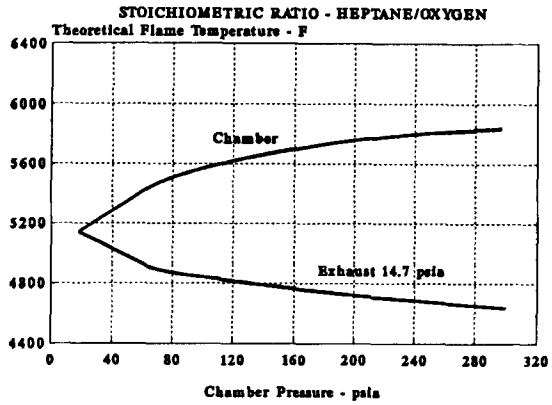

Figure 2 Variation of theoretical flame temperature and exhaust temperature with chamber pressure.

pressure in a confined chamber is 7.1 bar (105 psi) according to the perfect gas law. This is typical of a closed vessel that has a geometry that does not permit the detonation wave to develop, *i.e.*, a length/diameter ratio of 15 to 40.[3] At spark ignition, the subsonic flame front propagates down the barrel, developing into a supersonic detonation wave and producing a barrel full of hot (over 3482 °C, or 6300 °F), high pressure (10.2 bar, 150 psig) gas with suspended particles. The powder is then expelled along with the hot gas. Gas temperatures are higher because of pressure effects (Fig. 2) (calculated from Ref 4). Although instantaneous detonation pressures can be higher (Table 1),[5] Tucker[1] confirms that the actual D-Gun pressure is 10.2 bar (150 psig). Particle velocities will be a fraction (25 to 50%) of the exit gas velocities outside the nozzle (Fig. 3),[4] where adiabatic isentropic expansion is assumed.

The D-Gun can be considered an intermittent HVOF process. Because the detonation phenomenon physically limits the pressure rise in the combustion chamber (and therefore the particle velocity), the continuous burning HVOF process can increase chamber pressure over the D-Gun system and therefore can theoretically achieve higher particle velocity and coating quality. The only limits to a higher particle velocity in the HVOF process are the requirements to use higher oxidant and fuel pressures. The particle velocities obtained are a function of chamber pressure. In Fig. 4, it can be seen that the velocity of the gas, and therefore the particle velocity, increases with chamber pressure.

The relatively recent introduction of high-pressure, high-energy HVOF technology (Fig. 5) agrees with the preceding D-Gun description, in that 150 psig of chamber pressure permits continuous rather than intermittent application of coatings equal or superior to the D-Gun.[5] Availability of higher pressure HVOF equipment should broadly expand the field of HVOF applications.

Particle velocity (*i.e.*, the speed at which particles of coating material travel during their flight from the spray gun to the part being coated) is a critical factor in all thermal spray processes. Significantly, HVOF guns can produce particle velocities that are considerably higher than the other currently available commercial thermal spray processes.[1] Additionally, HVOF guns provide in-process protection of the powder particles from the time of injection in the gun, during the flight to the part, and at impact onto the substrate.

Specific particle conditions that contribute to the HVOF advantages compared with other types of thermal spray processes in open air include:

- Favorable environment
- Much shorter exposure time in flight
- Reduced mixing with ambient air once the jet and particles leave the gun
- Lower ultimate particle temperatures compared to plasma or arc guns
- Higher particle kinetic energy upon impact against the substrate

These HVOF characteristics translate into superior coating qualities, as summarized in Table 2.[5]

3. Designs to Generate High-Velocity Flames

The basic requirement of a HVOF system is to burn fuel and oxidant in an enclosed volume or chamber and build up pressure

Table 1 Pressure Rises from Flames and Detonations

Combustible mixture	Flame temperature	Detonation temperature	Constant volume pressure	
			Deflagration	Detonation
O_2/C_2H_2	3093 °C (5600 °F)	3482 °C (6300 °F)	7.1 bar (105 psig)	20 to 40 bar (300 to 600 psig)

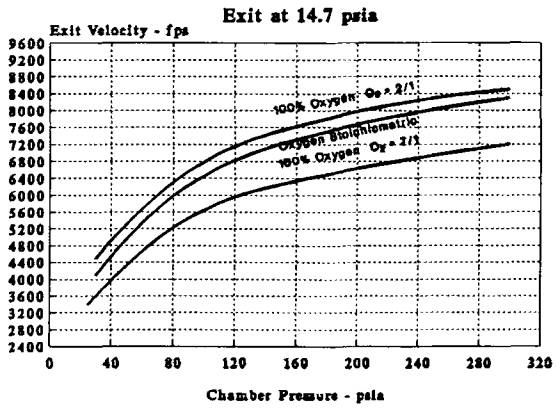

Figure 3 Variation of exit velocity with chamber pressure and oxygen/fuel ratio.

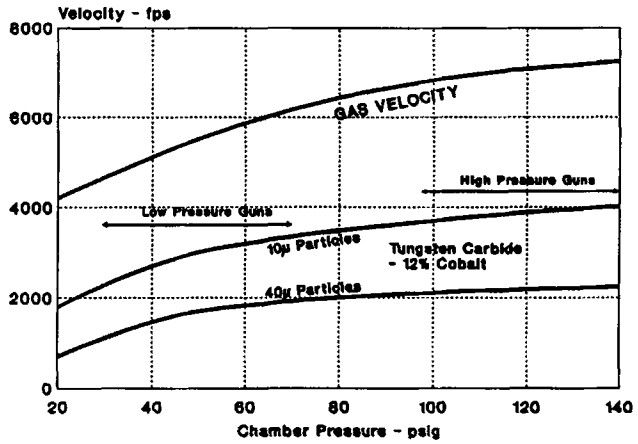

Figure 4 HVOF velocity versus gun pressure.

so that the gases expand through an orifice as they exhaust and accelerate to the atmosphere. A number of burner designs can be used to accomplish this, each having advantages and disadvantages, as detailed below.

3.1 *Throat Combustion Burners*

3.1.1 *Water-Cooled Burners*

Early in the 1950s, a significant amount of work was done by Smith[6] at Union Carbide, using a throat combustion system, Fig. 6(a). In this throat combustion burner, a cylindrical water-cooled barrel was used (no combustion chamber existed). The fuel and oxidant, in this case acetylene and oxygen, were injected at about 30 psig into a combustion region operating at a pressure of 25 psig,[7] which was maintained in the back end of the burner. Powder was injected axially, and the flow stream and particles accelerated in normal HVOF fashion.

The advantage of this system would appear to be simplicity and reduced burner chamber surface area and thus reduced heat losses. The thermal efficiency of such a device was in the range of 80%,[7] *i.e.*, approximately 80% of the input fuel energy leaves the exit nozzle as heat and kinetic energy. The disadvantage of this device is the limited throughput per unit area due to flame stabilization requirements (blow out) and therefore limited chamber pressure and lower exit velocity.

3.1.2 *Air-Cooled Burners*

A modification of the previous design is the air-cooled throat combustion system. Two versions exist—one a finned metal wall (similar to Fig. 6a) with compressed air cooling[8] and the second an air sheath unit shown in Fig. 6(b). In the latter, an annular flow of air between the chamber walls and the flame contains and constricts the flow and reduces wall heating. Significantly, air dilution of the combustion stream raises the oxygen level in the flow stream and thus increases the oxide content of the coating.[9-11] Furthermore, the air sheath produces additional turbulence and mixing, which decreases the flame temperature. The design, however, reduces the ability to use long barrels and thus limits particle velocity. Advantages of the design are its simplicity (no water-cooling passages) and low weight.

3.2 *Chamber Burners*

By using a larger diameter combustion chamber, throughput can be increased (higher blow out limits) and therefore chamber pressure and thus gas and particle velocity (Fig. 3) can be increased. The advantages of the chamber burner versus throat burner include higher particle velocity and more particle heating because of the longer barrel length without air entrainment.

3.2.1 *Right Angle/Central Injection*

The first type of chamber, Jet Kote,[12] shown in Fig. 6(c), uses a right-angled combustion system, in which the flame is burned in a larger diameter combustion chamber at right angles to the exit nozzle. This is an appealing design, especially for handheld guns. Most HVOF systems, however, are machine-mounted because of noise, heat, and thrust.

Table 2 HVOF Benefits

Coating benefit	Main causes
Higher density (lower porosity)	Higher impact energy
Improved corrosion barrier	Less through porosity
Higher hardness ratings	Less carbide degradation, better bond
Better wear resistance	Harder, tougher coating
Higher bond and cohesive strengths	Improved particle bonding
Fewer unmelted particle content	Better particle heating
Greater chemistry/phase retention	Reduced time at temperature
Thicker coatings (per pass and total)	Less residual stresses
Smoother as-sprayed surfaces	Higher impact energy

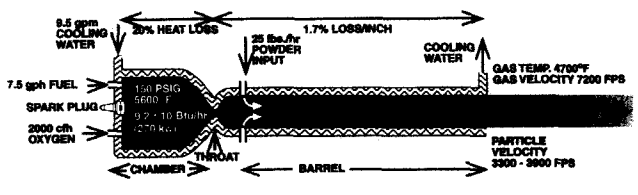

Figure 5 JP-5000 HP/HVOF system.

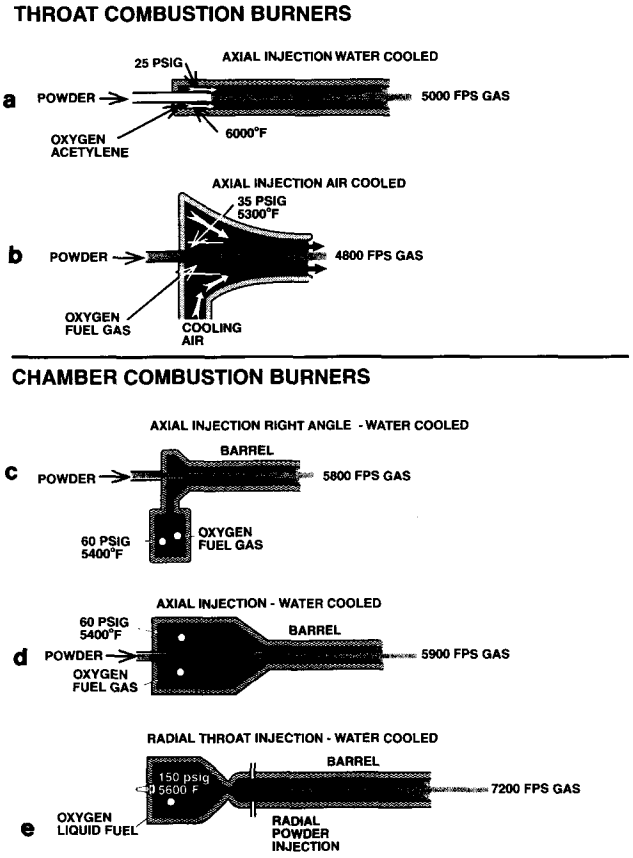

Figure 6 Evolution of HVOF spray guns.

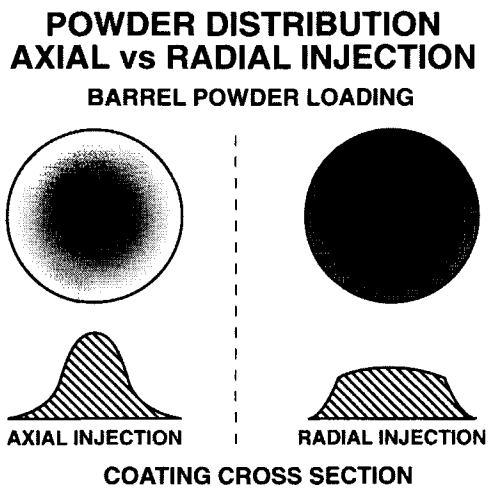

Figure 7 Powder distribution with two types of powder injection.

A distribution head at the exit of the combustion chamber, and prior to the exit barrel, directs the flow at 90° and provides a method of injecting the gases uniformly into the exit nozzle. This design also provides a water-cooled area for injecting powder on the axis of the gas stream in the throat region.

The disadvantages of this right-angled nozzle are additional heat losses of the immersed turning head and high differential heat fluxes, which can cause cracking. The nozzle design also extracts energy and cools the gas prior to injection of powder, thereby reducing the gas temperatures available for particle heating.

3.2.2 *Straight Through/Axial Injection*

An evolution of the water-cooled HVOF design is the axial flow device shown in Fig. 6(d). This incorporates central injection of powder within an axially located combustion chamber. This design improves thermal efficiency while providing central powder injection. It is envisioned that central injection of powder would permit more uniform heating of the particles, less critical injection parameters and therefore more uniformly heat-affected powder that may result in superior coatings.

3.2.3 *Straight Through/Radial Injection*

Figure 6(e) is a modification of the axial chamber system shown in Fig. 6(d). In this case, a converging/diverging nozzle is added, and the powder is injected beyond the throat (the smallest diameter in the system) at the beginning of the barrel. Because powder injection in HVOF jets is much different from conventional flame or plasma systems, it has been found that central injection does not provide the expected advantages.

As the combustion gases leave the combustion chamber and pass through the throat, an underexpanded condition then occurs, producing low pressure just downstream of the throat. Powder injected at this point provides simplified powder injection and containment and permits multiple-port powder injection, enabling more uniform loading of the exit stream and more efficient use of the available heat. This permits significantly higher spray rates per unit of energy input. Operating data show that at least twice the spray rate per unit of energy can be achieved with radial powder injection versus axial injection. The lower pressure powder injection region also alleviates the need (and cost) for a high-pressure powder feeder and canister.

Studies of powder loading in the central versus radial injection modes show that material is more uniformly distributed within the exit jet with radial injection, thus producing a flatter coating profile, which permits wider, less critical indexing (spacing) between passes. Figure 7 graphically shows a comparison of powder distribution and coating profile.

4. Theoretical

In this investigation, calculations were carried out on a specific HVOF gun design (JP-5000)[13] operating with a stoichiometric mixture of kerosene and oxygen, which is ignited and burned in a cylindrical combustion chamber. For these calculations, the pressure in the chamber is maintained at about 120 psig (9.27 bar) (Fig. 5). Intensive water cooling of the combustion chamber and the barrel is necessary. For a 6-in. long barrel (used in the following calculations), the cooling water absorbs 82.3 kW (2.8×10^5 Btu/hr) or 30.5% of the fuel heating value.

The combustion gases are expanded in a convergent-divergent nozzle to supersonic speed, then flow through a barrel which may be up to 12 in. long. Fine powders (10 to 50 μm, *e.g.*, carbides, metals or alloys) are injected into this supersonic stream through multiple ports at the gas entrance to the barrel (Fig. 5). This powder is turbulently mixed and accelerated to high speeds and heated within the barrel. The gas-powder mixture leaves the barrel as a high-velocity jet and is directed toward the surface to be coated.

For this analysis, it was assumed that the fuel was heptane rather than kerosene. Heptane is similar in its combustion properties to kerosene, but has the advantage that due to its simple composition (C_7H_{16}) the combustion, adiabatic flame temperature, and behavior of the off-gases can be easily analyzed.

4.1 *Gas Conditions*

The combustion was calculated with the program developed by Gordon and McBride.[4] The adiabatic flame temperature of the stoichiometric combustion gases at 9.27 bar (120 psig) is 3400 K (5660 °F). Flame and jet temperature also varies with the oxygen/fuel ratio. Because about 50 kW of heat is removed in the combustion chamber, the gases entering the converging-diverging nozzle are at a temperature of only 3190 K (5310 °F). This was considered to be the stagnation temperature. The gas expansion in the nozzle was assumed to be isentropic. Furthermore, it was assumed that the isentropic coefficient throughout the nozzle (evaluated from Ref 4) was constant.

The molar mass of the gas is, according to Ref 4:

$$M = 25.84 \text{ kg/kgmol}$$

with the given stagnation conditions of $T° = 3190$ K, $p° = 9.27$ bar, and an isentropic coefficient of $\gamma = 1.115$. The flow condition in the throat of the nozzle can be calculated and is denoted by an asterisk (*) for isentropic flow behavior and no further chemical reaction (frozen equilibrium flow):

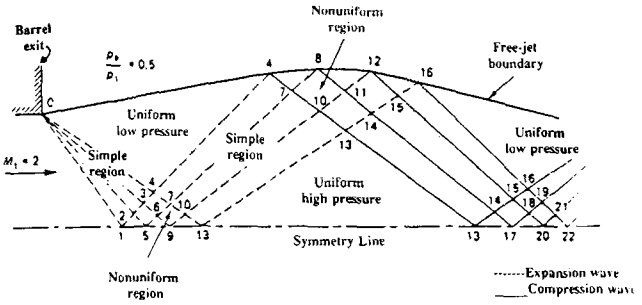

Figure 8 Shock formation of an underexpanded jet. From Saad[15]

$$T^* = T^\circ\left(\frac{2}{\gamma+1}\right) \quad T^* = 3015\,\text{K} \tag{1}$$

$$p^* = p^\circ\left(\frac{2}{\gamma+1}\right)^{\gamma/(\gamma-1)} \quad p^* = 5.39\,\text{bar} \tag{2}$$

$$\rho^* = \rho^\circ\left(\frac{2}{\gamma+1}\right)^{1/(\gamma-1)} \quad \rho^* = 0.55\,\text{kg/m}^3 \tag{3}$$

$$c^* = \sqrt{\gamma(\Re / \overline{M})T^*} \tag{4}$$

where $\Re$ is the universal gas constant ($\Re$ = 8.314 kJ/kg · mol · K). Thus, c^* = 1040 m/sec (3411 ft/sec).

For the flow rate of 28.4 l/hr (7.5 gal/hr) of heptane and 56,632 l/hr (2000 scf/hr) of oxygen, the overall mass flow rate is $\dot{m}_t$ = 0.0259 kg/sec.

Now the throat diameter (d) can be calculated, because:

$$\dot{m}_t = \rho^* c^* \times \frac{\pi d^2}{4} \quad d^* = 7.6 \times 10^{-3}\,\text{m} \tag{5}$$

which is very close to the experimental diameter used, *i.e.*, $\frac{5}{16}$ in. = 7.9×10^{-3} m.

Further expansion occurs in the divergent section of the nozzle (Fig. 5), where the diameter of the cross section increases from $d^* = \frac{5}{16}$ in. to $d^* = \frac{7}{16}$ in., thus the actual cross section increases by almost a factor of 2, and the speed of the gas increases to almost twice the local speed of sound. The Mach number at the exit of the diverging section of the nozzle, M_a, is[14]

$$\frac{d^2}{d^{*2}} = \frac{1}{M_a^2}\left(\frac{1 + (\gamma-1)/2M_a^2}{(\gamma+1)/2}\right)^{(\gamma+1)/[2(\gamma-1)]} \quad M_a = 1.98 \tag{6}$$

The temperature at the upstream entrance to the barrel is

$$T = T^\circ\left(1 + \frac{\gamma-1}{2}M_a^2\right)^{-1} \quad T = 2600\,\text{K}\ (4200\,^\circ\text{F}) \tag{7}$$

The pressure can be calculated as

$$p = p^\circ\left(\frac{T}{T^\circ}\right)^{[\gamma/(\gamma-1)]} \quad p = 1.3\,\text{bar} \tag{8}$$

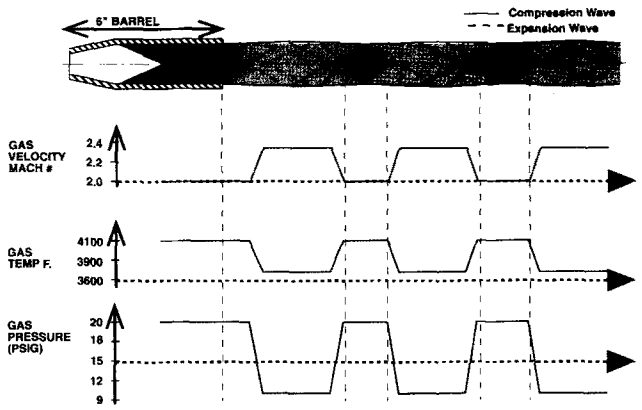

Figure 9 Shock diamond cross section, HVOF jet.

The value obtained in Eq 8 is similar to experimental measurements of 1.35 bar in this region.

The velocity of sound is

$$c = \sqrt{\gamma(\Re / \overline{M} \cdot T)} \quad c = 960\,\text{m/sec} \tag{9}$$

Thus, the actual gas velocity at the entrance to the barrel is

$$v = c M_a \quad v = 1900\,\text{m/sec} \tag{10}$$

and the gas density is

$$\rho = \rho\overline{M} / (\Re T) \quad \rho = 0.155\,\text{kg/m}^3 \tag{11}$$

Friction in the barrel slows the flow somewhat (see Ref 14). We assumed in a first-order analysis that the flow in the barrel is adiabatic and that no shock occurs. A weak shock occurs at the entrance to the barrel due to the fact that the flow changes its direction, but this shock is probably weakened by expansion waves from the nozzle. Friction results in a decrease in the gas velocity:[14]

$$\frac{dM_a^2}{M_a^2} = \gamma M_a^2 \cdot \frac{1 + (y-1)/2M_a^2}{1 - M_a^2}\ f\frac{dz}{d} \tag{12}$$

where f is the friction coefficient and z the coordinate along the length of the barrel. The flow is highly turbulent (Reynolds number, 2×10^7) and therefore f = 0.005 is a good first approximation. The Mach number at the exit of the barrel is obtained by numerical integration over the length of the barrel and is calculated to be M_a = 1.85.

The free stream pressure increases according to

$$\frac{dp}{p} = \gamma M_a^2 \frac{1 + (\gamma-1)/2M_a^2}{2(1 - M_a^2)}\ f\frac{dz}{d} \tag{13}$$

and at the exit it will be

$$p = 1.37\,\text{bar}$$

The sudden change in flow direction (pressure) from the divergent section of the nozzle to the barrel sets up a Prandt-Meyer

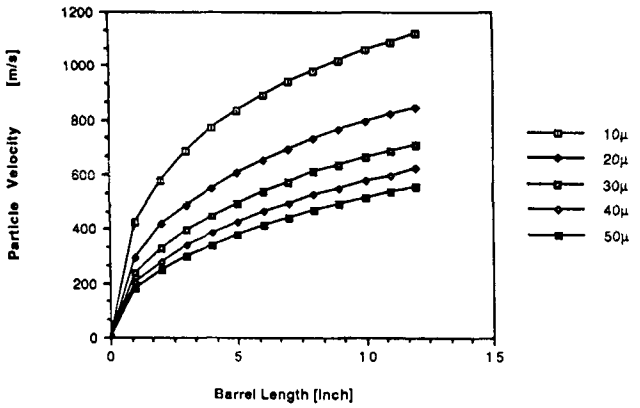

Figure 10 Effect of barrel length on exit particle velocity.

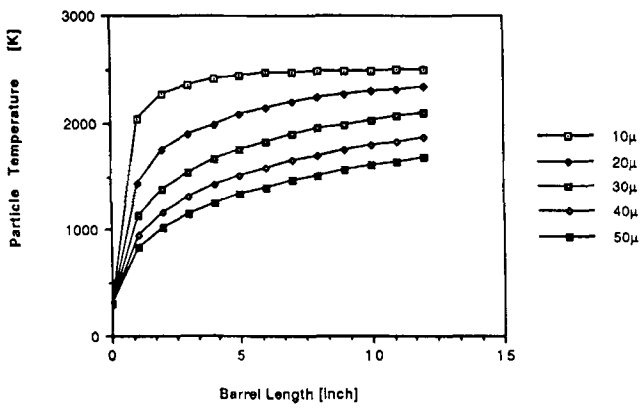

Figure 11 Effect of barrel length on exit particle temperature.

flow in the barrel (see Ref 15) which consists of weak expansion and compression waves. The flow pattern after the exit from the barrel is similar to that shown in Fig. 8.[15]

A simplified linear shock analysis for the flow in the free jet was carried out.[16,17] It is assumed that the flow is adiabatic and that the oblique shocks are weak such that entropy changes can be disregarded. The linearized theory permits relatively easy graphical solution. Only two shocks are shown in each case, even though a multiplicity is present, as indicated in Fig. 8.

Figure 9 shows the calculated shock flow pattern, temperature, pressure, and velocity (Mach number) variations in the flow with oblique shocks along the centerline (dash-dotted line). The cyclic changes of the flow would extend to infinity (infinite jet length) in the absence of friction and air entrainment, but in reality the oblique shock pattern will reduce the diameter and continue only until sufficient outside air is entrained into the jet so that the temperature and velocity of the jet have decreased substantially.

Such decay can be seen in actual jet photographs. One can observe the decrease in the diameter of the shock diamonds as one proceeds from the barrel exit. The diamonds are brighter because of greater pressure and therefore temperature in those regions. The flow at the exit from the barrel is supersonic, the pressure is above atmospheric, and thus the jet is underexpanded. Immediately after the exit, the jet overexpands, the pressure drops below atmospheric, and the increased velocity reduces temperature. In the above calculations, it was assumed that no particles were present in the flow.

It is interesting to note that the barrel, even after extended use, shows negligible erosion due to the injection of hard tungsten carbide particles. The powder injection can be adjusted such that the particles are suspended in the gas throughout the barrel. The weak shocks and turbulence do not alter the particle trajectory sufficiently for the particles to aggressively hit the wall.

4.2 *Effect on Particles*

The particles injected into the supersonic flow of the HVOF gun will experience (based on Newtonian flow) an acceleration:

$$\frac{dv_f}{dt} = \frac{3}{4} C_d \left[\frac{\rho_g}{\rho_f}\right] \frac{[(v_g - v_f)\, abs\, (v_g - v_f)]}{d} \qquad [14]$$

where ρ_f is the particle density, ρ_g is the gas density, v_f is the particle velocity, v_g is the gas velocity, d is the particle diameter, and C_d is the drag coefficient.

Because the particles are initially injected into a supersonic flow, each particle will have a shock wave on the upstream side. The drag induced on these particles in this supersonic flow, as calculated with the empirical correlation by Walsh,[18] is valid up to Mach 2. For low-velocity flow, the drag can be evaluated from well-known drag correlations.[19] The particles are assumed to have sufficient distance from each other, thus interaction was neglected, and the drag correlation for single particles was used.

A computer program was written using the assumptions described herein. The particles in the gas stream were assumed to be spherical. The empirical correlation for the drag coefficient was put into a polynomial form.[18] The drag coefficient calculated from this relation is only slightly larger than the drag coefficient evaluated from the well-known correlation at low velocities.

Heat transfer between the gas and the particles was described with the known relation for spheres:

$$Nu = 2 + 0.6 \times Re^{0.5} \times Pr^{0.33} \qquad [15]$$

since no heat transfer relation for particles exposed to supersonic flow was available. Note Nu = Nusselt number.

As described previously, the drag coefficient did not differ substantially for subsonic and supersonic flow. Thus, by analogy, the foregoing heat transfer relation is probably an adequate approximation for this first-order analysis. Neither friction nor oblique shocks in the barrel and in the free jet were considered in the subsequent calculations.

Figure 10 shows the calculated barrel exit velocity of tungsten carbide particles in the size range 10 to 50 μm as a function of barrel length. The temperature of the particles leaving the barrel was also calculated (Fig. 11). It was assumed that the particle properties are constant and that no melting occurs (an approximation). The gas temperature was taken as constant at $T = 2500$ K (4041 °F).

Figure 11 shows that the particles, even the larger ones, heat up very quickly. Tungsten carbide particles are usually mixed, agglomerated, or coated with cobalt. Cobalt has a melting point of about 1760 K (2637 °F). The results indicate that 40-μm and

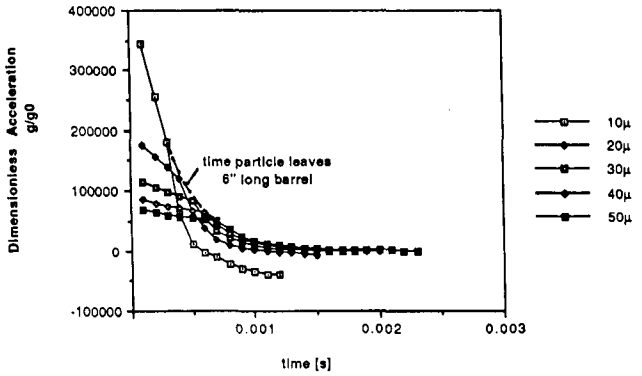

Figure 12 Dimensionless acceleration versus residence time in the gas jet.

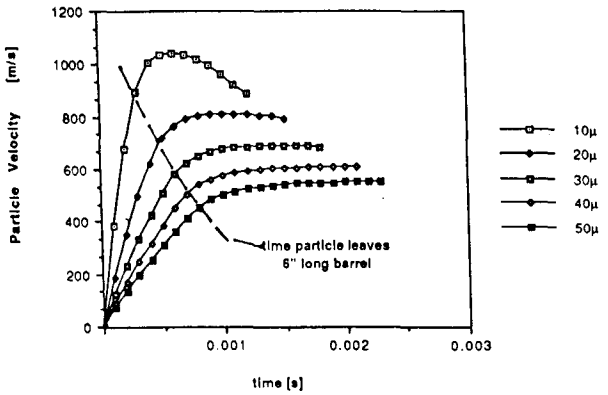

Figure 13 Particle velocity versus residence time in gas jet.

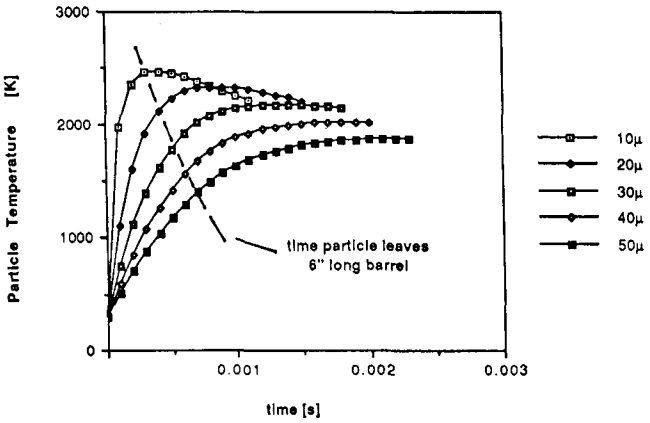

Figure 14 Particle temperature versus residence time in the gas jet.

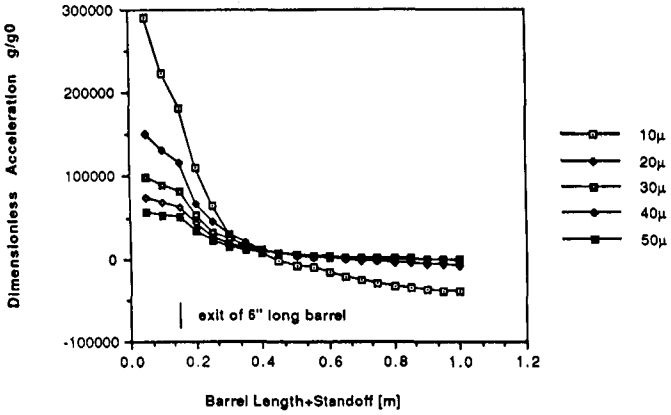

Figure 15 Dimensionless acceleration versus barrel + standoff length.

smaller particles reach that melting point before leaving an 8-in. barrel. The particle temperature will not change further (for coated particles) during the flight until all the cobalt coating is melted, because the heat of fusion must be provided by heat transfer. This is not considered in this simple analysis. For good bonding of the coating to the substrate, it is important that the cobalt is liquid or at least softened when the particles impact against the substrate.

Experimental observations confirm that 40-μm cobalt-coated tungsten carbide particles are sufficiently molten to adhere to the wall of the barrels of the HVOF described herein, at lengths beyond 8 to 10 in. This approximates the calculated data in Fig. 11, *i.e.*, the temperature of a 40-μm particle at 8 to 10 in. is about 1760 K (2637 °F).

After leaving the barrel, the high-velocity, high-temperature gas stream will entrain cold air from the environment and thus will spread, slow down, and cool. The shock diamonds become smaller further downstream and are observed to dissipate at about 20 diameters (0.22 m, or 8.75 in.) with the 8.2-bar (120-psig) HVOF system.

In the analysis, it was assumed that the overall gas momentum stayed constant. From Schlichting,[20] the maximum velocity in the center of the circular jet can then be calculated, but one should note that this model is not necessarily valid for supersonic flow. The maximum velocity is calculated from:

$$v_{max} = C\,C\,\frac{1}{z}\sqrt{\frac{J}{\rho}} \qquad [16]$$

where the momentum is $J = \int_0^\infty \rho v^2 2\pi r\, dr$ where r is the radius of the jet. In the calculations, it was assumed that all particles were exposed to this maximum centerline velocity.

Because J is a constant, we can find its value at the exit of the barrel:

$$J = \rho\, v^2 \pi r^2 \quad J = 54.27\ \text{N} \qquad [17]$$

The constant C can be found from the dimensions of the equipment as:

$$C = \frac{z}{r} \qquad [18]$$

A collimated powder stream was observed in this HVOF system with few hot particles in the boundary of the jet, thus lending credence to the assumption that all particles can be assumed to

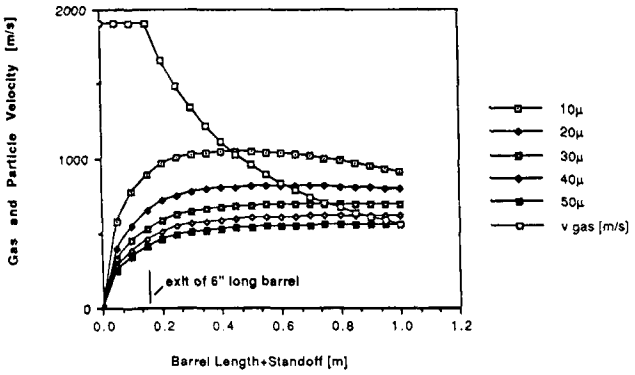

Figure 16 HVOF gas and particle velocity for 6-in. barrel.

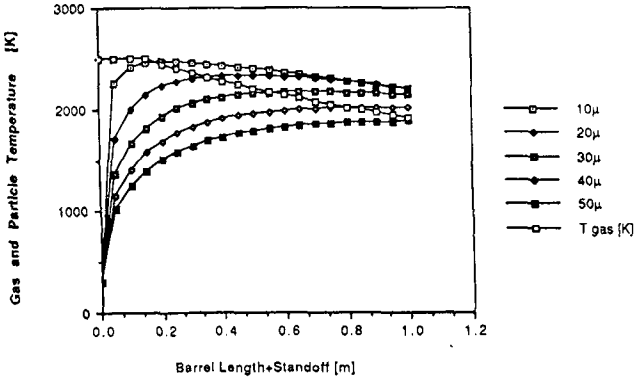

Figure 17 Gas and particle temperature for 6-in. barrel.

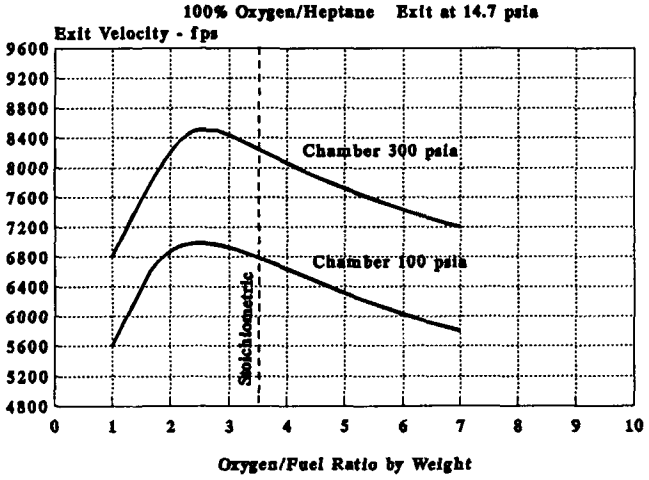

Figure 18 Variation of exit velocity with oxygen/fuel ratio.

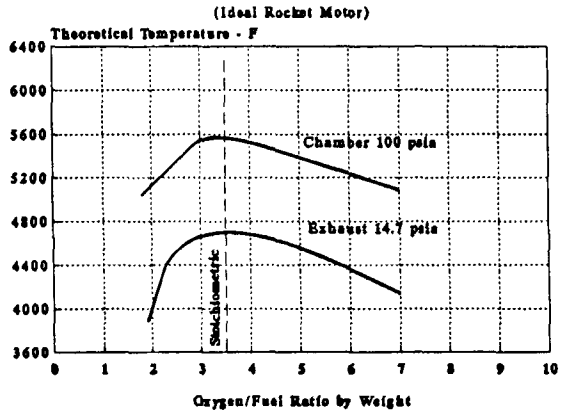

Figure 19 Variation of theoretical flame temperature with oxygen/fuel ratio.

remain in the jet in the coating standoff region of 10 to 20 in. The volume of the jet is[20]

$$Q = 0.404 \sqrt{\frac{J}{\rho}} z \qquad [19]$$

A mass and energy balance of the jet allows evaluation of the particle acceleration, velocity, and temperature. Results of these calculations for an HVOF gun with a 0.15-m (6-in.) long barrel are shown in Fig. 12 to 14.

The smaller particles achieve a higher velocity and thus hit the substrate sooner than the larger particles. Conversely, the process may be thought of as self-regulating; *i.e.*, large particles have a longer residence time and thus require more time to heat up (see Fig. 13 and 14). Significantly, only the smallest particles (10 μm) have a tendency to follow the decaying gas velocity and temperature after leaving the barrel (Fig. 16 and 17, respectively).

Figures 15 through 17 show the same sequence, but this time dimensionless acceleration, particle velocity, and particle temperature are plotted against distance traveled (1 m). Note that all but the largest particles (not usually sprayed) have a velocity higher than the gas velocity when hitting the substrate. The same is true for the temperature. This explains why satisfactory coatings are achieved with a 1-m stand off, because particle temperature and velocity are almost constant from 0.25 to 1 m.

4.3 *Other Considerations*

The previous calculations assumed a stoichiometric oxygen/fuel ratio. Oxygen/fuel ratio influences gas temperature, exit velocity and therefore particle melting capability, particle velocity, and ultimately coating quality. An understanding of such combustion-related properties is helpful in interpreting coating results. Figures 18 and 19 show how jet velocity and temperature are affected by the oxygen/fuel ratio.[4] Maximum velocities are achieved in the stoichiometric to slightly fuel-lean range (Fig. 18) and decays significantly (13 to 15%) in highly fuel-rich and fuel-lean regions.

Also, thrust (or impulse) from HVOF systems varies with throughput, oxygen/fuel ratio, and chamber pressure. Figure 20 can be used to calculate the thrust (force) produced by the burner. Typically, the HVOF unit shown in Fig. 5 burns about 0.058 lb/sec of gases and produces a calculated thrust of 14 lb. Note that the thrust measurement can be used to compare practi-

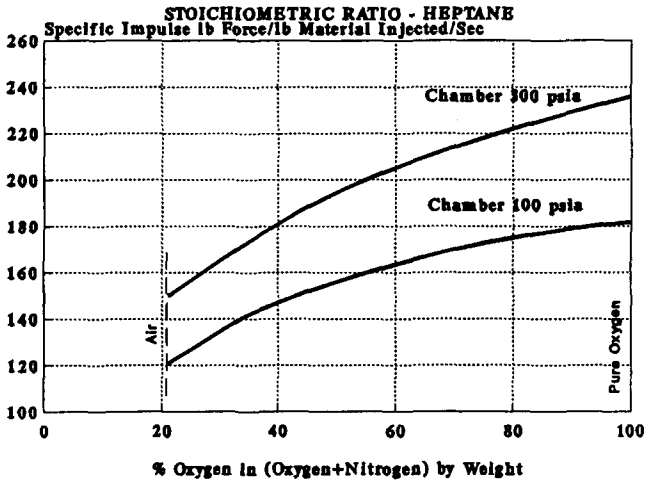

Figure 20 Variation of specific impulse with oxygen enrichment.

cal and theoretical results and thus compare combustion efficiency changes with burner design modifications.

5. Conclusion

A theoretical analysis of a 120-psig chamber pressure commercial design was profiled. Gas and particle temperatures and velocities, pressures, and Mach numbers have been calculated and plotted at various points within the gun and spray stream. Significantly, all measured parameters were in close agreement with calculated and predicted values. Flow patterns and shock-wave phenomena have also been described and compared with actual observations.

The gas velocity of a 120-psig chamber pressure HVOF torch, inside the exit of a 0.15-m (6-in.) barrel (1.36 bar, 20 psig), is about twice the velocity of sound, namely 1900 m/sec (6200 ft/sec). This corresponds to about five times the velocity of sound in air at ambient temperature and 1 atm. Note that the gas velocity beyond the exit shock of the barrel increases to a theoretical velocity of 2200 m/sec (7200 ft/sec) (Fig. 3 and 9).

The jet is underexpanded. The calculations and heat balance show that due to friction in the 6-in. long barrel, the temperature of the gas will increase by about 60 °C (132 °F), but intensive water cooling will cool it by approximately 180 °C (356 °F). Furthermore, the temperature of the gas decreases, due to heating of the injected powder in the barrel, but this is only in the range of 10 °C if about 3.8 g/sec (30 lb/hr) of powder are injected into the flow. Thus, the temperature at the exit of the barrel will be about 140 °C (2840 °F) cooler than at the entrance and thus will be about 2500 K (4149 °F).

According to this simplified analysis, only the smallest particles are accelerated to velocities in excess of 900 m/sec (2952 ft/sec) in the barrel. However, particles continue to accelerate beyond the exit of the barrel, with the smallest particles (10 μm) reaching 1050 m/sec (3444 ft/sec) at 6 in. standoff (55% of maximum gas velocity), whereas 50-μm particles reach 500 m/sec (1640 ft/sec) (26% of gas velocity). Currently, 20- to 50-

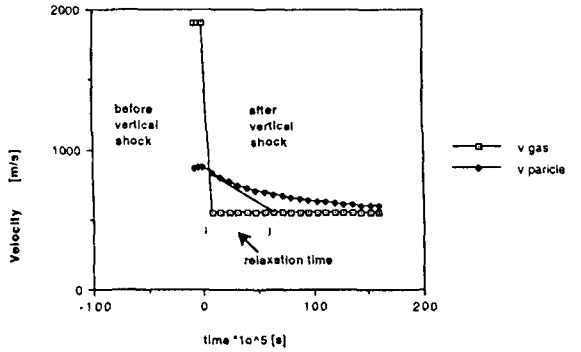

Figure 21 Relaxation of particle traveling through a vertical shock.

μm particles are normally used in this process. The exact particle velocities can only be evaluated if the complicated gas flow in the barrel and the oblique shocks are considered. In an exact analysis, the relaxation of particles has to be included—that is the time particles need to adjust to a different temperature or velocity field. An example of such a relaxation is shown in Fig. 21 for a particle exposed to a vertical shock.

The quantitative results obtained in this very simple analysis should be considered with some caution. However, they seem to explain observed phenomenon to a remarkable degree. Theory predicts that 40-μm particles of cobalt will reach their melting point at the exit of the 8-in. gun barrel. Experimental results confirm this. Theory also predicts that particles continue at maximum velocity and temperature 1 m from the barrel exit. Coating quality at 1 m confirms this. Again theory predicts an underexpanded jet beyond the throat and at the barrel exit. Pressure measurements and visual observations confirm this.

Particle velocity measurements by Smith[21] confirm our predictions, *e.g.*, that heavy particles like tungsten carbide maintain a high velocity of extended distances (0.5 m) from the nozzle. It should be noted however that much lighter particles (Al_2O_3) behave dramatically different.

A number of HVOF systems have evolved during the last 9 years. The principles of various HVOF gun designs have been reviewed and a detailed analysis of one design (JP-5000) has been given. This and other such fundamental data should provide a useful basis for greater understanding of HVOF principles and contribute to the design of more advanced thermal spray equipment.

References

1. A. Brown, "Spraying for Strength," *Aerospace America*, 52-53, Jan (1992).
2. T.C. McGeary and J.M. Koffskey, "Engineering Applications for Flame Plating," *Met. Prog.*, 80-86, Jan (1965).
3. L.A. Medard, *Accidental Explosions*, Vol. 1, John Wiley & Sons, New York, 311 (1989).
4. S. Gordon and B. McBride, "Computer Program for Calculation of Complex Chemical Equilibrium Compositions,...," NASA SP-273, Mar (1976), new version 1989.
5. Hobart Tafa Technologies, Inc., Technical Bulletin 1.3.1.2, Mar (1992).

6. U.S. Patent 2,861,900, issued 11/25/58, A. Smith, J. Pelton, R. Eschenbach.
7. R. Eschenbach, RETECH INC., personal communication, Nov (1991).
8. U.S. Patent 4,634,611, issued 1/6/87, J. Browning.
9. R. Kaufold, A. Rotolico, J. Nerz, and B. Kushner, "Deposition of Coatings Using a New High Velocity Combustion Spray Gun," NTSC Proceedings, May 20, ASM International, 561-569 (1990).
10. D.J. Varacalle, A.J. Rotolico, *et al.*, "HVOF Combustion Spraying of Inconel Powder," ITSC'92 Proceedings, ASM International, Table 3, June (1992).
11. G.C. Irons, "The Benefits of Higher Velocity Thermal Spray Guns," NTSC '91 Proceedings, ASM International, May (1991).
12. U.S. Patent 4,568,019, issued 2/4/86, J. Browning.
13. Hobart Tafa Technologies, Inc., Technical Bulletin 1.3.2.2.4, Feb (1992).
14. F.M. White, *Fluid Mechanics*, McGraw-Hill, New York (1986).
15. M.A. Saad, *Compressible Fluid Flow*, Prentice-Hall, Englewood Cliffs, NJ (1985).
16. A. Shapiro, *The Dynamics and Thermodynamics of Compressible Fluid Flow*, Vol. I and II, Ronald Press, New York (1953).
17. R. Courant and K.O. Friedrichs, *Supersonic Flows and Shock Waves*, Interscience Publishers, New York (1953).
18. M.J. Walsh, "Drag Coefficient Equations for Small Particles in High Speed Flows," *American Institute of Aeromautics and Astromautics Journal, 13*(11), 1526-1528 (1975).
19. G.B. Wallis, *One Dimensional Two-Phase Flow*, McGraw-Hill, New York (1969).
20. H. Schlichting, *Boundary Layer Theory*, McGraw-Hill, New York (1960).
21. M. Smith, W. Oberkampf, K. Kowalsky, and D. Marantz, "HVOF: Particle, Flame Diagnostics and Coating Characteristics," NTSC Proceedings, May 20, ASM International, 587-592 (1990).